

Published in IET Control Theory and Applications
 Received on 24th July 2008
 Revised on 22nd January 2009
 doi: 10.1049/iet-cta.2008.0317



H_∞ disturbance observer design for high precision track following in hard disk drives

C.K. Thum^{1,2} C. Du² F.L. Lewis³ B.M. Chen¹ E.H. Ong²

¹Department of Electrical and Computer Engineering, National University of Singapore, Singapore 117576, Singapore

²A*STAR Data Storage Institute, No. 5, Engineering Drive 1 (off Kent Ridge Crescent), Singapore 117608, Singapore

³Advanced Controls and Sensors Group, Automation and Robotics Research Institute, The University of Texas at Arlington, Arlington, TX 76019, USA

E-mail: ckthum@nus.edu.sg

Abstract: Contrary to the conventional method of disturbance observers (DOB) where Q -filter is designed to be a low-pass filter with unity DC gain, the optimal H_∞ method has been proposed to design the Q -filter and applied in the servo control system of hard disk drives in track following. Simulation and implementation results have shown that the resultant H_∞ DOB improves low-frequency disturbance attenuation without compromising the disturbances attenuation performance at higher frequency region achieved by the nominal feedback controller. In terms of track-following precision, the proposed method is approximately 5% more accurate than the conventional method.

1 Introduction

The servomechanism is a major component of the hard disk drive (HDD), which is responsible of increasing the storage capacity by means of increasing the track density, measured by track-per-inch (TPI). As TPI increases annually, the effect of disturbances from various track misregistration contributors, namely flex cable bias, airflow-induced disk, suspension and slider vibrations as well as spindle non-repeatable runout (NRRO), become more and more significant.

The idea of observing disturbance to improve the performance of servomechanism was firstly introduced in [1]. It was suggested that if the disturbances were supposedly generated by a linear dynamic system and the model of the system was known, they could be estimated from the system's output measurements by an asymptotic estimator (Luenberger observer) and the effect of the disturbances could be neutralised by feeding the disturbance estimates back into the system [2, 3]. Over the years, the method has been modified and applied. However, it is not always easy to identify the disturbance model. Further, it is not always true to assume that disturbance model is linear time invariant (LTI). Several years later since then, a new type of disturbance observer

(DOB) had been introduced [4]. This new method does not require control designers to have the full information of the disturbance model and assume it to be LTI. However, it requires the model of controlled plant to be accurately known and invertible, at least within the bandwidth of interest [5]. Recently, it has been proven that under certain assumptions imposed on the plant and disturbance models, the two different methods are equivalent in that the original DOB introduced in [1] is actually a generalisation of the latter method [6]. In this paper, we focus on the latter method.

It has already been shown that a DOB is capable of estimating disturbances and modelling error [4, 5]. Further, as no additional sensors are required and it can be easily implemented in an 'add-on' fashion that requires minimal change to the existing feedback controller of the HDD servo system, the DOB provides a cheap and easy solution to help HDD servo control designers to push up TPI. Hence, since its introduction, a number of applications of DOB in the HDD servo systems have been proposed, such as that in [5] where DOB is used to enhance the attenuation effectiveness to shock and vibration, in [7] where a DOB with the low-pass Q -filter designed using stochastic estimation theory and corporately implemented

with an accelerometer is used to compensate pivot friction, in [8] where the DOB with accelerator measurement is applied to perform selective disturbance compensation in real time, and in [9] where the narrowband disturbance is further attenuated using a DOB with the Q -filter designed to be a bandpass filter such that it is approximately unity in the narrow frequency band. In [10], an H_∞ method is involved in the design of Q -filter. However, the structure of the Q -filter was proposed to be fixed and the method made use of the result of [6] to design the parameters of low-pass Q -filter with unity DC gain using H_∞ control theory. Consequently, the performance of that method is comparable to that of the conventional method.

Bounded by the Bode Integral Theorem, the sensitivity gain function cannot be improved at all frequencies. Thus in this paper, we propose an alternative designing approach based on H_∞ optimal control theory, in which the Q -filter with a general form is designed systematically and flexibly using performance weight functions. It is then applied in the servo control of HDD in track following to pursue high precision positioning. Simulation and implementation results will show that the proposed method can improve low-frequency disturbances attenuation while not compromising the excellent disturbances attenuation at higher frequencies achieved by the nominal feedback controller.

2 Proposed DOB Design

This section aims to derive a new approach of designing a DOB based on H_∞ optimal control theory [11]. In this section, all transfer functions are expressed in the discrete-time domain for digital design and implementation.

2.1 DOB with nominal feedback controller

Fig. 1 shows the block diagram of a DOB with the nominal feedback controller, where y , n , v , u_q and u represent the controlled output, disturbance, measurement noise, the estimated disturbance and the total control input, respectively. P represents the actuator plant. Its nominal transfer function, P_0 , can be obtained using the method

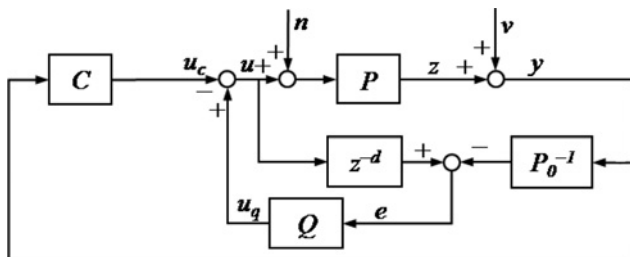


Figure 1 Block diagram of DOB with the nominal feedback controller

in [12] and expressed as

$$P_0(z^{-1}) = \frac{z^{-d}B(z^{-1})}{A(z^{-1})} \quad (1)$$

where $A(z^{-1}) = 1 + a_1z^{-1} + \dots + a_nz^{-n}$ and $B(z^{-1}) = b_0 + b_1z^{-1} + \dots + b_mz^{-m}$. In Fig. 1, C is the nominal feedback controller that is designed to achieve nominal servo performance and stability.

Assuming that the sampling frequency is much higher than the system bandwidth, within the bandwidth of interest $P_0 \approx P$ [13] and the effect of z^{-d} is small. It can be derived from Fig. 1 that

$$z \approx SP(1 - Q)n - T(1 - Q)v - Qv \quad (2)$$

where S and T are, respectively, the sensitivity function and the complementary sensitivity function of the nominal feedback loop, which are given by

$$S = \frac{1}{1 + PC} \quad \text{and} \quad T = 1 - S \quad (3)$$

Consequently, it becomes apparent that the block diagram in Fig. 1 can be approximately simplified as in Fig. 2. In Fig. 2, n_c and v_c represents the controlled effect of, respectively, n and v with the nominal feedback control loop.

Remark 1: After the simplification, we can see that the design of the outer nominal feedback loop and the inner DOB feedback loop are completely decoupled from each other. Effects of the nominal feedback loop are seen as feedforward signals by the DOB feedback loop. This makes the design process of the add-on DOB more intuitive and straightforward.

In Fig. 2, given that C has been properly designed such that the nominal control loop has a good attenuation to

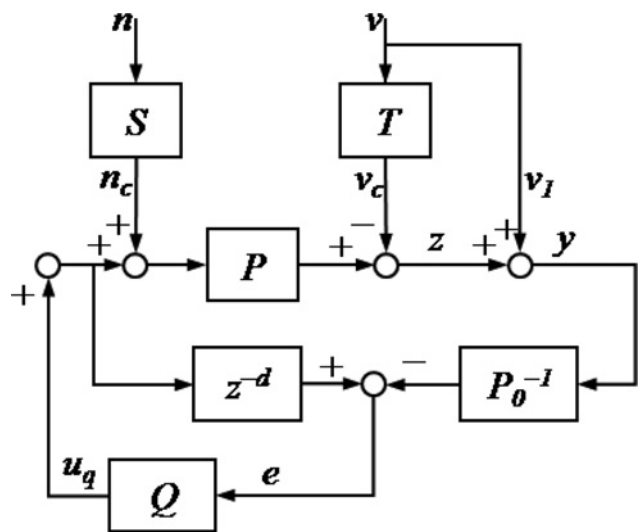


Figure 2 Approximately simplified block diagram of Fig. 1

measurement noise v , we can assume v_c is negligible compared to the effect on z from n_c and v_1 . This is possible since $|T|$ becomes less than 1 in a much broader frequency range after the closed-loop bandwidth, say around 1 kHz with a high sampling rate of 40 kHz. Hence we can formulate the design problem of Q that minimises the weighted effect of n and v_1 on the error signal z into a standard H_∞ problem, that is

$$\text{minimise } \|W_n T_{zn} \quad W_v T_{zv_1}\|_\infty \quad (4)$$

where W_n and W_v are stable weighting functions, and T_{zn} and T_{zv_1} represents respectively, the transfer functions from n to z and from v_1 to z .

2.2 H_∞ Q-filter design

Introducing the following state-space representation of Q

$$x_q(k+1) = A_q x_q(k) + B_q e(k) \quad (5)$$

$$u_q(k) = C_q x_q(k) + D_q e(k) \quad (6)$$

Denote (A_p, B_p, C_p, D_p) and (A_i, B_i, C_i, D_i) as the state-space realisation of P and P_0^{-1} respectively, and (A_n, B_n, C_n, D_n) and (A_v, B_v, C_v, D_v) as the state-space realisation of $W_n S$ and W_v , respectively. (A_a, B_a, C_a, D_a) stands for the state-space realisation of z^{-d} .

Ignoring v_c , from Fig. 2, we have

$$x(k+1) = Ax(k) + B_1 w(k) + B_2 u_q(k) \quad (7)$$

$$e(k) = C_1 x(k) + D_{11} w(k) + D_{12} u_q(k) \quad (8)$$

$$z(k) = C_2 x(k) + D_{21} w(k) + D_{22} u_q(k) \quad (9)$$

where

$$A = \begin{bmatrix} A_p & B_p C_n & 0 & 0 & 0 \\ 0 & A_n & 0 & 0 & 0 \\ 0 & 0 & A_v & 0 & 0 \\ 0 & 0 & 0 & A_a & 0 \\ B_i C_p & 0 & B_i C_v & 0 & A_i \end{bmatrix}$$

$$B_1 = \begin{bmatrix} B_p D_n & 0 \\ B_n & 0 \\ 0 & B_v \\ 0 & 0 \\ 0 & B_i D_v \end{bmatrix}, B_2 = \begin{bmatrix} B_p \\ 0 \\ 0 \\ B_a \\ B_i D_p \end{bmatrix}$$

$$C_1 = [-D_i C_p \quad -D_i D_p C_n \quad -D_i C_v \quad C_a \quad -C_i]$$

$$C_2 = [C_p \quad D_p C_n \quad 0 \quad 0 \quad 0]$$

$$D_{11} = [-D_i D_p D_n \quad -D_i D_v], D_{12} = D_a - D_i D_p$$

$$D_{21} = [D_p D_n \quad 0], D_{22} = D_p$$

$$\text{and } w = [n \quad v_1]$$

Associated with (7)–(9), our objective is to design a dynamic Q -filter with the general form of (5)–(6), such that (4) is achieved. It is known that (A_q, B_q, C_q, D_q) in (5)–(6) can be easily obtained using either the H_∞ -algebraic riccati equation (ARE) method [11, 14] or the H_∞ -linear matrix inequality (LMI) method [15, 16].

3 Application to a HDD servo system

We proceed to design a DOB for a HDD using our proposed method. Implementation results will be given and compared with those of using conventional DOB designing method.

3.1 Disk drive modelling

Fig. 3 shows the typical picture of the 3.5" HDD with a Voice Coil Motor (VCM) actuator that will be used for in our experiment. It consists of a stack of flat rotating disks with position (servo) information embedded on their surfaces. Position error signal (PES) calculated from the servo information is used to measure the position the R/W heads.

The model of the plant to be controlled, that is, the VCM actuator mounted with the suspension is obtained by system input-output identification. In this paper, during our implementation, instead of using the servo information, the position measurement of the plant is obtained using a Polytec OFV 3001S Scanning Laser Doppler Vibrometer (LDV) in the range of $2 \mu\text{m/V}$. A dynamic signal analyser is used to generate a swept sine signal to excite the actuator so as to capture the frequency response of the dynamics of the actuator in frequency domain. Fig. 4 shows the measured frequency response of the actuator and its nominal model.

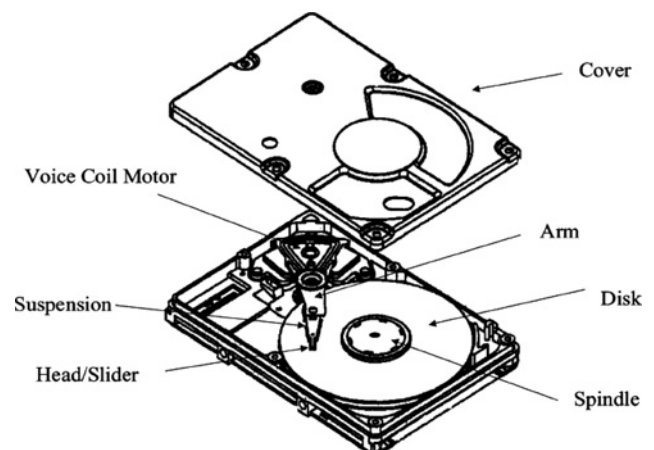


Figure 3 HDD with a VCM actuator

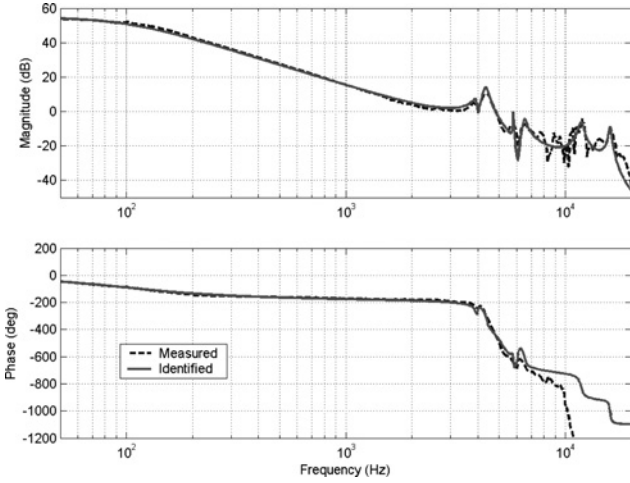


Figure 4 Frequency responses of the VCM actuator (LDV range: 2 μm/V)

The 16th-order nominal plant model of the actuator is obtained using the curve-fitting technique that approximates the measured frequency responses. Its transfer function is given by

$$P(s) = \frac{2.18000 \times 10^8}{s^2 + 1005.00s + 3.94800 \times 10^5} P^d(s) \prod_{i=1}^6 P_i^{rm}(s) \quad (10)$$

with six main resonance modes given by

$$P_1^{rm}(s) = \frac{0.970225s^2 + 487.688s + 6.12847 \times 10^8}{s^2 + 990.230s + 6.12847 \times 10^8} \quad (11)$$

$$P_2^{rm}(s) = \frac{0.562500s^2 + 819.956s + 7.47030 \times 10^8}{s^2 + 1366.59s + 7.47030 \times 10^8} \quad (12)$$

$$P_3^{rm}(s) = \frac{0.910020s^2 + 695.284s + 1.32805 \times 10^9}{s^2 + 364.425s + 1.32805 \times 10^9} \quad (13)$$

$$P_4^{rm}(s) = \frac{1.15074s^2 - 7.95337 \times 10^4s + 5.49697 \times 10^9}{s^2 + 3410.51s + 5.49697 \times 10^9} \quad (14)$$

$$P_5^{rm}(s) = \frac{1.16870s^2 + 1.73891 \times 10^5s + 1.01065 \times 10^{10}}{s^2 + 2010.61s + 1.01065 \times 10^{10}} \quad (15)$$

$$P_6^{rm}(s) = \frac{1.66796 \times 10^9}{s^2 + 1633.62s + 1.66796 \times 10^9} \quad (16)$$

and $P^d(s)$ is an all pass filter included to model any phase lag caused by system delay

$$P^d(s) = \frac{s^2 - 6534.51s + 1.06750 \times 10^9}{s^2 + 6534.51s + 1.06750 \times 10^9} \quad (17)$$

The NRRO disturbance and noise models used in this paper

are obtained from our servo track writing (STW) platform [17], which can be used to approximate the actual NRRO disturbance model inside any typical HDD. The disturbance distribution obtained from our STW platform is reflected in the measured PES NRRO power spectrum in Fig. 5, where the disturbances in the low frequencies (less than 200 Hz) are mostly due to external vibrations and windage, the narrowband NRRO at 650 Hz is due to disk vibration, and the 3.8 kHz are caused by the excited suspension resonance.

3.2 Designs of nominal feedback controller $C(z^{-1})$ and DOB

Next, we proceed to design a servo control system for the HDD with the models given above. From this point onwards, all transfer functions are expressed in the discrete time-domain for digital design and implementation

Prior to any controller design, the plant is precompensated with three second-order notch filters, namely F_1^{nf} , F_2^{nf} and F_3^{nf} , which are given by

$$F_1^{nf}(z^{-1}) = \frac{0.7895 - 1.223z^{-1} + 0.7564z^{-2}}{1 - 1.223z^{-1} + 0.546z^{-2}} \quad (18)$$

$$F_2^{nf}(z^{-1}) = \frac{0.6161 + 0.9356z^{-1} + 0.5433z^{-2}}{1 + 0.8105z^{-1} + 0.2846z^{-2}} \quad (19)$$

and

$$F_3^{nf}(z^{-1}) = \frac{0.6819 + 0.4013z^{-1} + 0.6206z^{-2}}{1 + 0.3141z^{-1} + 0.3897z^{-2}} \quad (20)$$

After the precompensation, the discretised model of $P(s)$ in

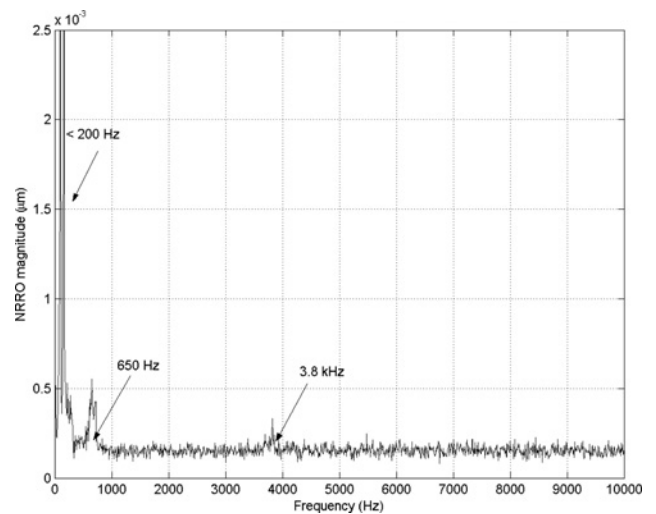


Figure 5 Measured NRRO power spectrum of the STW platform prior to servo control

(10) can be approximated by the second-order model

$$P_{\text{comp}}(z^{-1}) = F_1^{\text{nf}}(z^{-1})F_2^{\text{nf}}(z^{-1})F_3^{\text{nf}}(z^{-1})P(z^{-1}) \approx z^{-d} \frac{0.06766 + 0.0672z^{-1}}{1 - 1.98z^{-1} + 0.9798z^{-2}} \quad (21)$$

where $d = 1$.

Following our design method, the dynamic order of P_0^{-1} in Fig. 1 will be equal to the order of the discretised plant to be controlled, thus for a lower order controller, it is wise to use the precompensated plant in (2), which has a lower order than the zero-order-hold equivalent of the full plant model in (10). Consequently, P_0^{-1} is designed as

$$P_0^{-1}(z^{-1}) = \frac{1 - 1.98z^{-1} + 0.9798z^{-2}}{0.06766 + 0.0672z^{-1}} \quad (22)$$

The nominal feedback controller, C , has been designed to achieve nominal servo stability and performance. It is in the form of a lead-lag compensator and is given by

$$C(z^{-1}) = \frac{0.8314 - 1.611z^{-1} + 0.7808z^{-2}}{1 - 1.119z^{-1} + 0.12z^{-2}} \quad (23)$$

Here we expect the insertion of DOB will further improve disturbance attenuation at frequencies below 700 Hz. Thus, we design the weighting functions W_n and W_v to be, respectively, given by

$$W_n = 0.088 \text{ and } W_v = 0.9 \quad (24)$$

such that $|W_v| > |W_n P|$ at frequencies above 700 Hz typically.

Following the method described in Section 3 and MATLAB's *LMI Control Toolbox* [18], a Q -filter, Q_{prop} , which has been designed using the proposed method and reduced using MATLAB's *balmr* to a second-order discrete filter is given by

$$Q_{\text{prop.}}(z^{-1}) = \frac{0.094629 - 0.094184z^{-1}}{1 - 1.9012z^{-1} + 0.9017z^{-2}} \quad (25)$$

Its frequency response is shown in Fig. 6

For performance comparison, another Q -filter, $Q_{\text{conv.}}$, has been designed using the conventional method [4] whose frequency response is shown in Fig. 6. It is a low-pass, second-order Butterworth discrete filter with a cutoff frequency of 900 Hz and given by

$$Q_{\text{conv.}}(z^{-1}) = \frac{0.004536 + 0.009072z^{-1} + 0.004536z^{-2}}{1 - 1.8006z^{-1} + 0.8188z^{-2}} \quad (26)$$

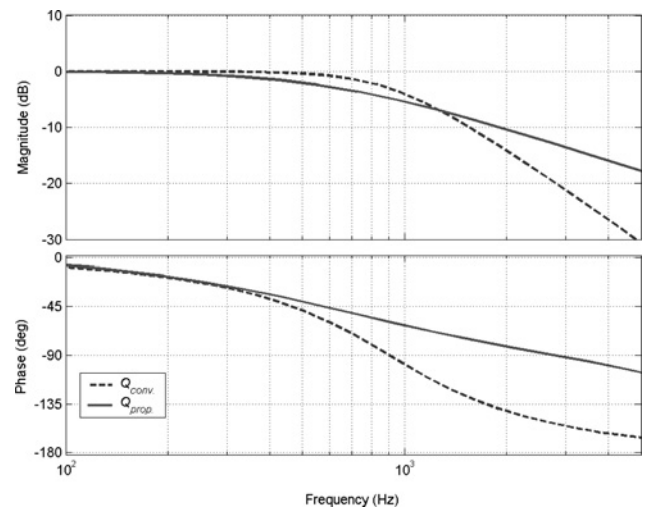


Figure 6 Frequency responses of respective Q -filters

From Fig. 6, it is apparent that the -3 dB bandwidth of $Q_{\text{conv.}}$ is smaller to that of $Q_{\text{prop.}}$.

From Fig. 2

$$T_{zn_c} = \frac{(1 - Qz^{-d})PP_0}{P_0 + Q(P - P_0z^{-d})} \quad (27)$$

This implies, ignoring the phase effect of z^{-d} and difference between P_0 and P , attenuation of n_c will take place in frequency region where $|1 - Q| < 1$ and amplification of n_c will take place in frequency region where $|1 - Q| > 1$.

Now, we devise a pictorial illustration, as shown in Fig. 7, to discuss the attenuation of n_c with DOB. As discussed earlier, the amplification of n_c will take place in the frequency region where $|1 - Q| > 1$ or $|Q - 1| > 1$. This implies the amplification of n_c happens where the Nyquist plot of $Q - 1$ leaves the unit circle $|z|$. From Fig. 6, it is noted that as the phase of $Q_{\text{conv.}}$ drops below -60° at

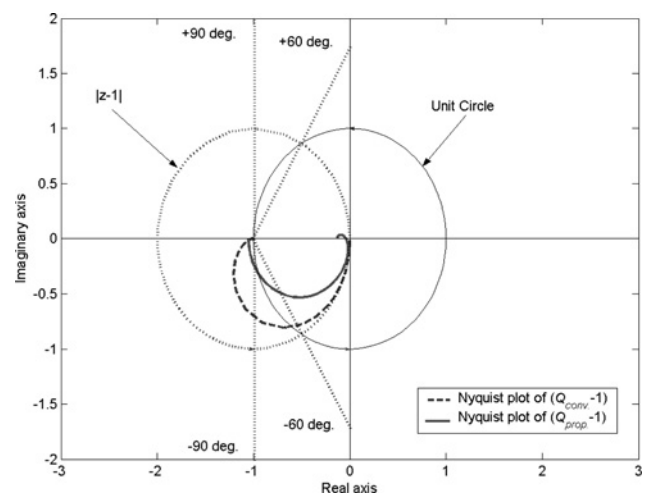


Figure 7 Illustration of attenuation of n_c with DOB using Nyquist plots of $(Q_{\text{conv.}} - 1)$ and $(Q_{\text{prop.}} - 1)$

approximately 660 Hz, because gain of $Q_{conv.}$ is not significantly smaller than unity and thus $|1 - Q| > 1$ as illustrated in Fig. 7, significant amplification of n_c may take place. On the other hand, when the phase of $Q_{prop.}$ reaches -60° $|Q_{prop.}| < -5$ dB and its gain steadily reduces to -12 dB as its phase drops to -90° . Hence, significant amplification of n_c will not happen with the proposed method. As seen in Fig. 7, the Nyquist plot of $(Q_{prop} - 1)$ stays inside the unit circle at most frequencies.

3.3 Simulation and implementation results

The experimental setup is shown in Fig. 8, where a dissected HDD is placed on a vibration free platform, the displacement of the R/W head is measured with a scanning LDV. All continuous-time models in this section is discretised using bilinear rule at a sampling frequency of 40 kHz for digital control design. All final digital controllers are implemented via a dSpace DSP installed on a desktop PC at this frequency.

Prior to experiments, Matlab simulations are conducted to verify the performance and stability robustness of the proposed design method against modelling error. The stability margins of the outer feedback loop, which are achieved by C , may be degraded with the addition of DOB. To analyse the stability of the final closed loop in Fig. 1, the transfer function T_{yu_c} from u_c to y is taken as a new plant, which is actually P that has been compensated by the DOB. The open loop transfer function CT_{yu_c} [5] is given by

$$T_{ol} = \frac{PP_0C}{P_0 + Q(P - P_0z^{-d})} \quad (28)$$

The simulated Nyquist plots for the nominal and perturbed plants are shown in Fig. 9. In terms of $\pm 10\%$ variations in the damping and frequency of plant resonances in (11)–(3.1) and in the coefficients of P^d in (17), the nominal feedback loop maintains stable with sufficient gain and phase margins as shown in Fig. 9. We have also analysed its

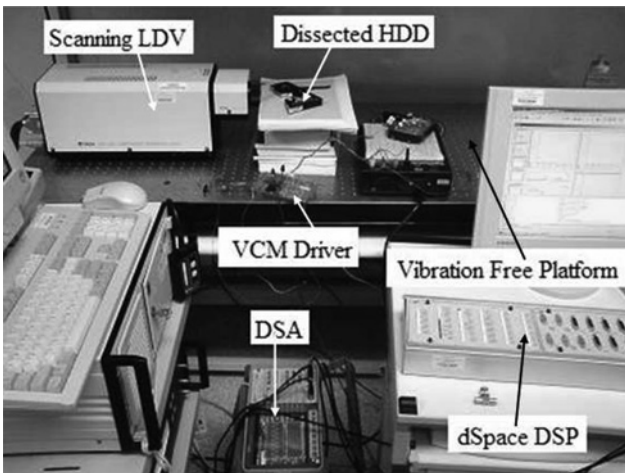


Figure 8 The experimental setup

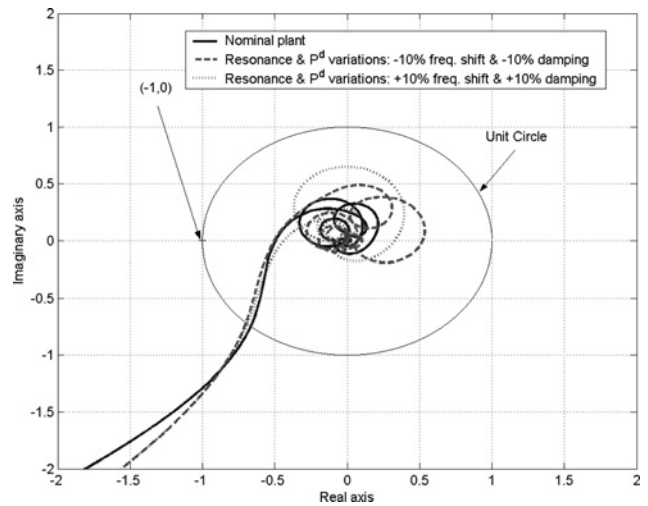


Figure 9 Nyquist plot of T_{ol} in (28) for the nominal and perturbed plant with $Q_{prop.}$

Gain margin: 8.5 dB (Nominal), 6.5 dB (-10% perturbation), 7 dB ($+10\%$ perturbation)
Phase margin: 50° (Nominal), 45° (-10% perturbation), 47° ($+10\%$ perturbation)

performance robustness against plant variations as well. Fig. 10 displays the sensitivity gain function for the nominal and perturbed plants, with the proposed designed DOB. From these figures, it is apparent that the proposed method is generally immune to reasonable plant variations.

The implementation results are shown as follows. Figs. 11–13 show the measured frequency responses of T_{ol} in (28) with and without DOB. From these figures, it is apparent that using a DOB with its Q -filter designed using either the conventional or the proposed method does not significantly worsen the stability margins of the nominal feedback achieved by C in (23) together with notch filters (18)–(20).

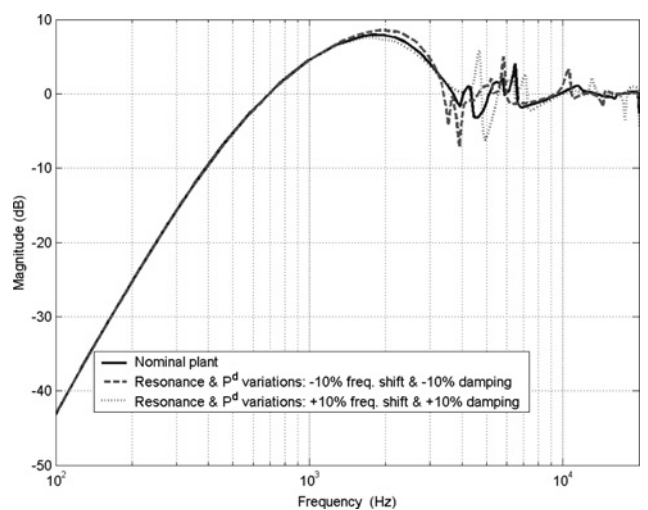


Figure 10 Simulated sensitivity gain for the nominal and perturbed plant with $Q_{prop.}$

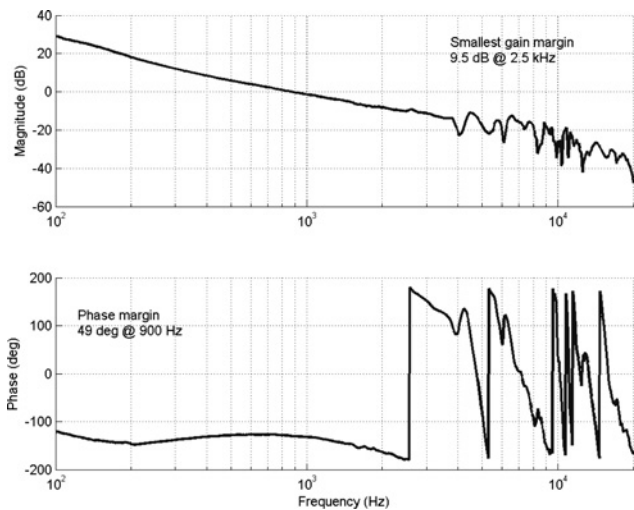


Figure 11 Open loop frequency responses with the nominal feedback controller C without DOB

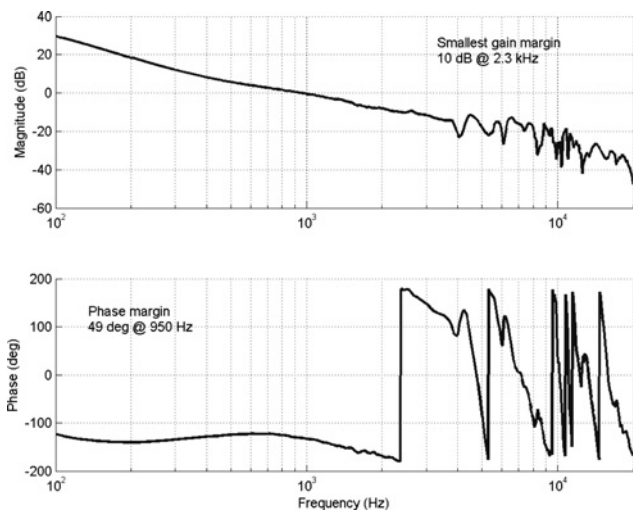


Figure 12 Frequency responses of T_{ol} with DOB designed using the conventional method, Q_{conv} .

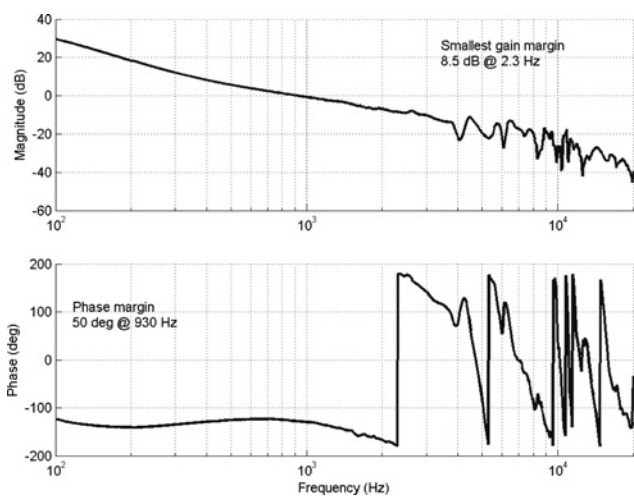


Figure 13 Frequency responses of T_{ol} with DOB designed using the proposed method, Q_{prop} .

Fig. 14 shows the measured gain of the sensitivity transfer function. While DOB designed using the conventional method helps to achieve more gain reduction at 500 Hz and below, the amount of gain reduction between 500 Hz and 4 kHz is reduced. The overall servo bandwidth is reduced from 800 to 630 Hz. As a result, more low frequencies disturbances that are located below 200 Hz are attenuated, the amount of attenuation for disturbances that centres around 650 Hz is slightly reduced. Unlike with the proposed method, the overall servo bandwidth is maintained unchanged at 800 Hz.

The NRRO with the spectrum in Fig. 5 is added into the closed loop during our experiment using dSpace. Consistently with the sensitivity function in Fig. 14, the measured NRRO power spectrum comparison is shown in Fig. 15. In terms of track-following accuracy, the

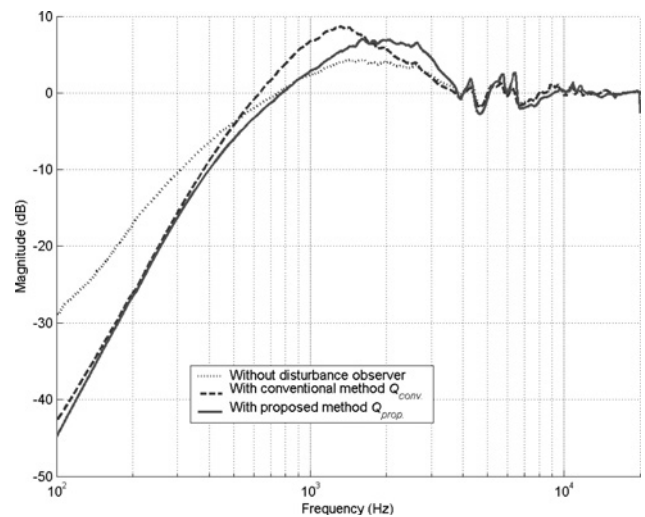


Figure 14 Measured gain of the sensitivity transfer function

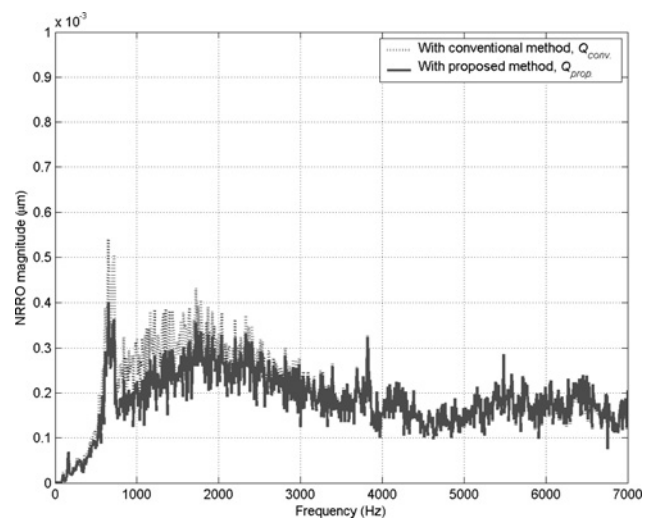


Figure 15 Power spectrum of measured PES NRRO with respective methods

conventional method manages to reduce the 3σ (standard deviation) value of the true PES NRRO from 11.5 to 10.9 nm, thus achieving approximately 6% more reduction. On the other hand, the proposed method has achieved a 3σ value of 10.3 nm. This implies the proposed method is about 5% more accurate than the conventional method during track-following.

4 Conclusion

In this paper, an H_∞ control theory approach to design a DOB has been considered. The block diagram of the standard DOB with nominal feedback has been simplified to facilitate H_∞ problem formulation. With the proposed method, while improving low-frequency disturbance attenuation, there is virtually no compromise on the higher frequency disturbance attenuation performance achieved by the nominal feedback controller. Implementation results have verified its effectiveness. Comparing to the conventional method, the proposed method manages to achieve approximately 5% more accuracy during track-following.

5 References

- [1] JOHNSON C.: 'Accommodation of external disturbances in linear regulator and servomechanism problems', *IEEE Trans. Autom. Control*, 1971, **163**, (6), pp. 635–644
- [2] DAVISON E.: 'The robust decentralized control of a general servomechanism problem', *IEEE Trans. Autom. Control*, 1976, **21**, (1), pp. 14–24
- [3] LEVIN JR. V., KREINDLER E.: 'Use of disturbance estimator for disturbance suppression', *IEEE Trans. Autom. Control*, 1976, **21**, (1), pp. 776–778
- [4] OHNISHI K.: 'A new servo method in mechatronics', *Trans. Jpn. Soc. Elect. Eng.*, 1987, **107-D**, pp. 83–86
- [5] WHITE M.T., TOMIZUKA M., SMITH C.: 'Improved track following in magnetic disk drives using a disturbance observer', *IEEE-ASME Trans. Mechatronics*, 2000, **5**, (1), pp. 3–11
- [6] SCHRIJVER E., VAN DIJK J.: 'Disturbance observers for rigid mechanical systems: equivalence, stability, and design', *ASME J. Dyn. Syst., Meas. Control*, 2002, **124**, pp. 539–548
- [7] ISHIKAWA J., TOMIZUKA M.: 'Pivot friction compensation using an accelerometer and a disturbance observer for hard disk drives', *IEEE-ASME Trans. Mechatronics*, 1998, **3**, (3), pp. 194–201
- [8] PARK S.-W., YANG H.S., PARK T.-W., PARK Y.-P.: 'Disturbance observer design for enhanced track following using accelerometer in HDD'. Proc. Asia Pacific Magnetic Recording Conf. (APMRC), August 2004, pp. 52–53
- [9] SEMBA T.: 'A disturbance observer to suppress vibration effects of a HDD in a disk array system'. Proc. American Control Conf., June 2003, pp. 1362–1367
- [10] WANG C.-C., TOMIZUKA M.: 'Design of robustly stable disturbance observers based on closed loop consideration using H_∞ optimization and its applications to motion control systems'. Proc. American Control Conf., 2004, pp. 3764–3769
- [11] ZHOU K., DOYLE J.C., GLOVER K.: 'Robust and optimal control' (Prentice-Hall Inc., New Jersey, 1996)
- [12] TOMIZUKA M.: 'Zero phase error tracking algorithm for digital control', *ASME J. Dyn. Syst., Meas. Control*, 1994, **116**, pp. 33–38
- [13] FRANKLIN G.F., POWELL J.D., WORKMAN M.L.: 'Digital control of dynamic systems' (Prentice Hall, Reading, 1997, 3rd edn.)
- [14] CHEN B.M., LEE T.H., PENG K., VENKATARAMANAN V.: 'Hard disk drive servo systems' (Springer, New York, 2006, 2nd edn.)
- [15] DE OLIVEIRA M. C., GEROMEL J.C., BERNUSSOU J.: 'An LMI optimization approach to multiobjective controller design for discrete-time systems'. Proc. IEEE Conf. on Decision and Control, 1999, vol. 4, pp. 3611–3616
- [16] DU C., GUO G.: 'Lowering the hump of sensitivity functions for discrete-time dual stage systems', *IEEE Trans. Control Syst. Technol.*, 2005, **13**, (5), pp. 791–797
- [17] DU C., XIE L., GUO G., ZHANG J., LI Q., HREDZAK B., TEOH J.N.: 'A generalized KYP lemma based control design and application for 425 kTPI servo track writing'. Proc. American Control Conf., 2006, pp. 1303–1308
- [18] GAHINET P., NEMIROVSKI A., LAUB A.J., CHILALI M.: 'LMI control toolbox' (The MathWorks, Inc., Natick, MA, 1995)